ACS OMEGA

http://pubs.acs.org/journal/acsodf

Article

Selective Allowance of Precipitation from Oversaturated Solution Using Surface Structures

Kihwan Kim, Kwangseok Lee, Jaehyun Choi, Jeong-Won Lee,* and Woonbong Hwang*

Cite This: *ACS Omega* 2022, 7, 987−993

Read Online

ACCESS | Metrics & More | Article Recommendations | Supporting Information

ABSTRACT: Precipitation is a well-known phenomenon commonly observed in salt ponds. However, it causes pipe clogging in industrial sites, which can be resolved by controlling the direction of precipitation. Herein, we propose a method to control the precipitation direction by changing the structures and properties of the solid surface. Bare, nanostructured, microstructured, and micro/nanostructured surfaces were immersed in the same saturated aqueous NaCl solution, and the heights at which precipitation occurred in the different specimens were compared. On bare and nanostructured surfaces, NaCl deposits as a flat layer on the surface, while on micro and micro/nanostructured surfaces, it forms a thick deposit in a direction perpendicular to the surface. When the same experiment was conducted on surfaces made by patterning different structural surfaces, the precipitates did not spread on the surface with microscale structures. We believe that this novel approach may prove useful in solving the problems caused by precipitation.

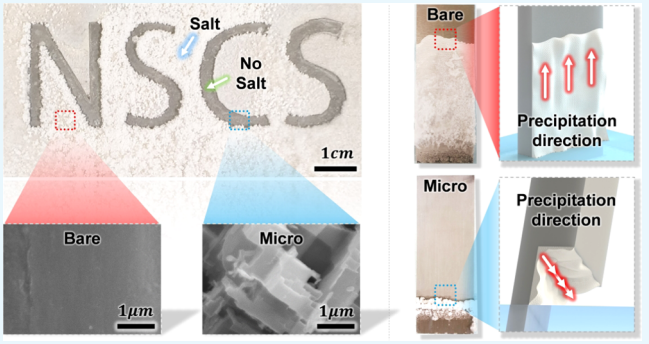

INTRODUCTION

The phenomenon of precipitation is widely used for both salt production and lithium production from salt ponds and salt lakes.[1−3] While precipitation is highly beneficial for salt and lithium production, it can also cause chronic pipe clogging.[4,5] Clogging of pipes may reduce the efficiency of heat exchangers or even block common pipe flow, resulting in significant losses.[6,7] Therefore, many researchers have investigated various ways to prevent precipitation.[8−10]

Precipitation is a chemical reaction that causes solid particles to separate from a liquid. The crystal size of the precipitates is influenced by the surface energy and temperature of the liquid.[11] The surface energy between solids and liquids is closely related to surface wettability, the extent of which is given by the contact angle (CA), i.e., the angle formed by a liquid droplet on a solid surface. The CA is determined by the interplay between the surface energies of the gas, liquid, and solid under thermodynamic equilibrium, and it decreases with increasing roughness, in accordance with the Wenzel state.[12,13]

Many researchers have investigated methods to control surface wettability by modifying surface energy and surface roughness.[14−20] In particular, surface modification has been used to improve the efficiency of condensation heat transfer by applying an antifrosting mechanism in heat exchangers.[21,22]

There have been many studies to learn more about controlling the liquefaction and formation of solids in gas; however, there has been little research on the inhibition and/or induction of precipitation utilizing the roughness of a surface. Herein, we propose a method to control the precipitation direction by changing the structure and properties of the solid surface. To the best of our knowledge, this is the first study on how to actively control the area of precipitation in an environment where precipitation is bound to occur. In this study, we also closely investigate the growth of precipitates and propose a new method to solve the problem of precipitation in pipelines.

RESULTS AND DISCUSSION

Principle of Nucleation. For precipitation to occur, it is imperative for the liquid to be oversaturated. The crystal nuclei are first generated in the liquid or on the surrounding surface. Precipitation in the liquid is known as homogeneous nucleation, while that on the surrounding surface is known as heterogeneous nucleation. For homogeneous nucleation (Figure S1), the Gibbs free energy change after crystallization can be determined by the following equation

$$\text{Gibbs free energy change} = -V_S(G_v^L - G_v^S) + A_{SL}\gamma_{SL} \quad (1)$$

where V_S is the solid volume, G_v^L and G_v^S are the Gibbs free energies per unit volume of the liquid and solid states,

Received: October 6, 2021
Accepted: December 23, 2021
Published: January 3, 2022

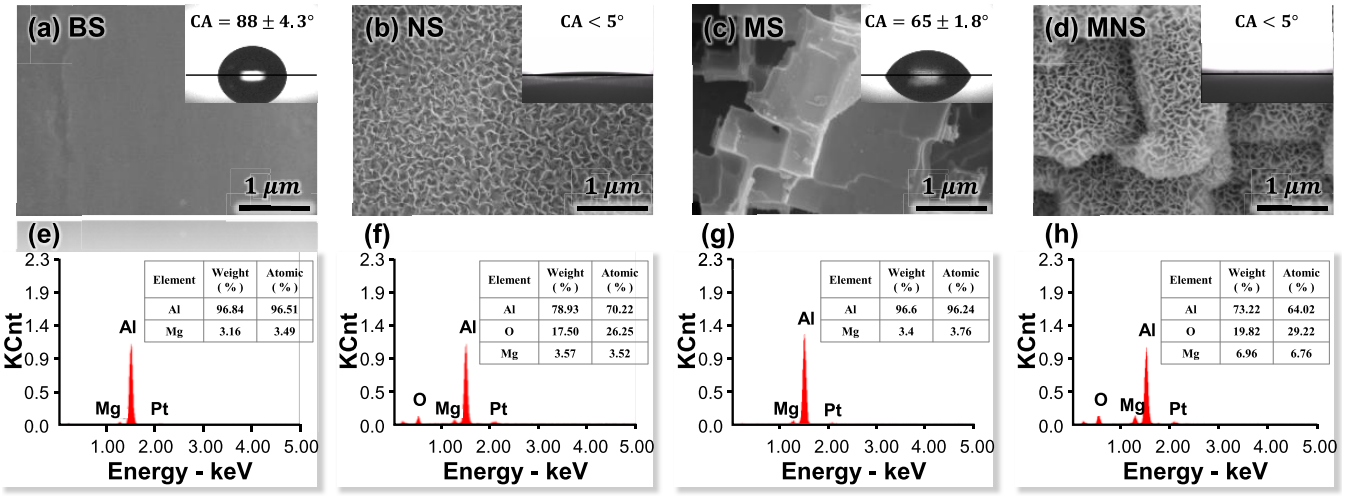

Figure 1. Characterization of various surfaces. Scanning electron microscopy (SEM) image and water contact angles (WCAs) of (a) bare surface, (b) nanostructured surface, (c) microstructured surface, and (d) micro/nanostructured surface. Energy-dispersive spectroscopy (EDS) results of (e) bare surface, (f) nanostructured surface, (g) microstructured surface, and (h) micro/nanostructured surface.

respectively, A_{SL} is the surface area between the solid and liquid phases, and γ_{SL} is the surface tension between the solid and liquid phases.[23] The Gibbs free energy difference can be determined by assuming the radius of the generated nucleus as r and using the following equation

$$\Delta G_v = (G_v^L - G_v^S),\ V_S = \frac{4}{3}\pi r^3 \text{ and } A_{SL} = 4\pi r^2 \tag{2}$$

$$\text{Gibbs free energy change } \Delta G(r) = -\frac{4}{3}\pi r^3 \Delta G_v + 4\pi r^2 \gamma_{SL} \tag{3}$$

where ΔG_v is the difference in the Gibbs free energy per unit volume between the liquid and the solid. To determine the critical radius r^* from the maximum change in Gibbs free energy, the value of r is calculated at the local maximum by differentiating $\Delta G(r)$ with respect to r.[24]

$$\frac{d(\Delta G(r))}{dr} = -4\pi r^2 \Delta G_v + 8\pi r \gamma_{SL} \tag{4}$$

$$-4\pi r^{*2} \Delta G_v + 8\pi r \times \gamma_{SL} = 0 \tag{5}$$

The theoretical critical homogeneous nucleation radius (r^*) and the homogeneous Gibbs free energy change (ΔG^*_{hom}) can be obtained as follows

$$r^* = \frac{2\gamma_{SL}}{\Delta G_v},\ \Delta G^*_{hom} = \frac{16\pi\gamma_{SL}^3}{3(\Delta G_v)^2} \tag{6}$$

If the radius of the generated nucleus is less than r^*, the Gibbs free energy may decrease as the nucleus redissolves. If it is larger than r^*, the Gibbs free energy may decrease as the nucleus grows. The change in Gibbs free energy for heterogeneous nucleation (Figure S2) can be determined using the following equation

$$\Delta G^*_{het} = \frac{16\pi\gamma_{SL}^3}{3\Delta G_v^2} \times S(\theta),\ S(\theta) = \frac{2 - 3\cos\theta + \cos^3\theta}{4} \tag{7}$$

where ΔG^*_{het} is the Gibbs free energy change for heterogeneous nucleation, which is related to the homogeneous nucleation as follows

$$\Delta G^*_{het} = \Delta G^*_{hom} \times S(\theta) \tag{8}$$

where $S(\theta)$ is <1. The Gibbs free energy change for heterogeneous nucleation is greater than that for homogeneous nucleation. In addition, the former occurs more spontaneously than the latter. Therefore, for our experiment, we induced salt precipitation on the aluminum surface, a heterogeneous surface, and analyzed the precipitation behavior.

Principle of the Capillary Phenomenon. When a capillary tube is placed in a liquid, the level of liquid in the tube becomes higher or lower than that outside the tube, which is called the capillary phenomenon. The height of the liquid in the tube is determined by the attraction between the molecules and that between the molecule and the wall of the tube. The level of liquid in the capillary tube can be determined as follows

$$h = \frac{2\gamma\cos(\theta)}{\rho r g} \tag{9}$$

where γ is the surface tension of the liquid, θ is the contact angle, ρ is the density of the liquid, r is the radius of the capillary tube, and g is the gravitational acceleration.[25] According to eq 9, the smaller the radius of the tube, the greater is the height of liquid in the tube.

Characterization of Aluminum Surfaces. The structure of each surface was observed by scanning electron microscopy (SEM), and the results are shown in Figure 1. The bare surface (BS) has a clean surface (Figure 1a), while the nanostructured surface (NS) has a structure comprising nanoflakes (Figure 1b). The microcubic structure is well-formed on both microstructured surfaces (MS) and micro/nanostructured surface (MNS) (Figure 1c,d, respectively). The approximate structure sizes of the NS and MS are 100 nm and 1 μm, respectively. Only Al and Mg components were detected when the surface components were analyzed by energy-dispersive spectrometry (EDS) because an aluminum oxide film was formed on both BS and MS (Figure 1e–g). In contrast, an aluminum hydroxide layer was formed on NS and MNS,

https://doi.org/10.1021/acsomega.1c05572
ACS Omega 2022, 7, 987−993

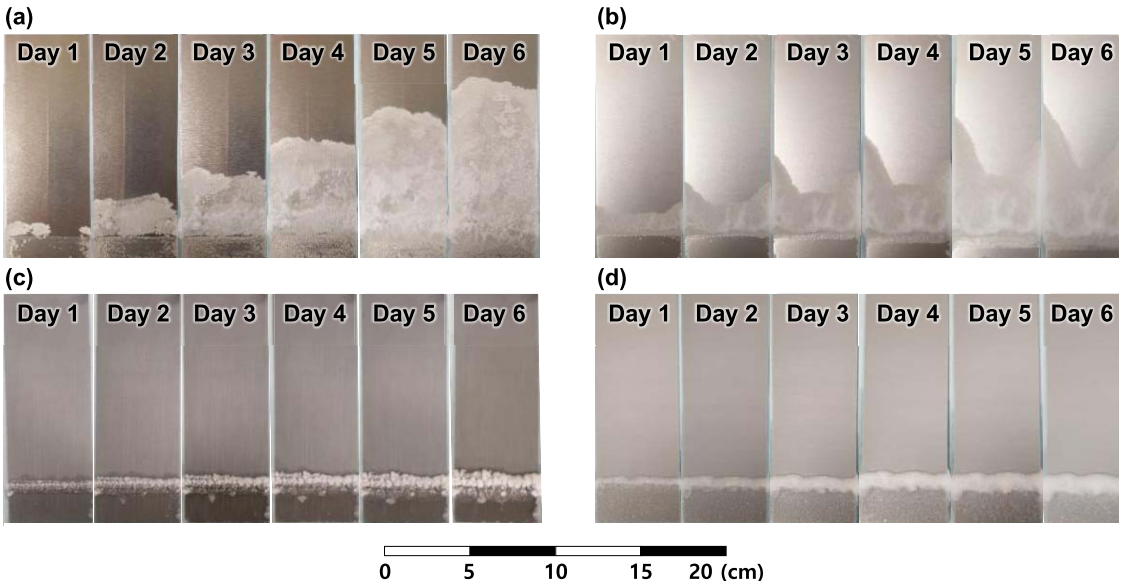

Figure 2. Results of the precipitation experiment over time. (a) Bare surface, (b) nanostructured surface, (c) microstructured surface, and (d) micro/nanostructured surface.

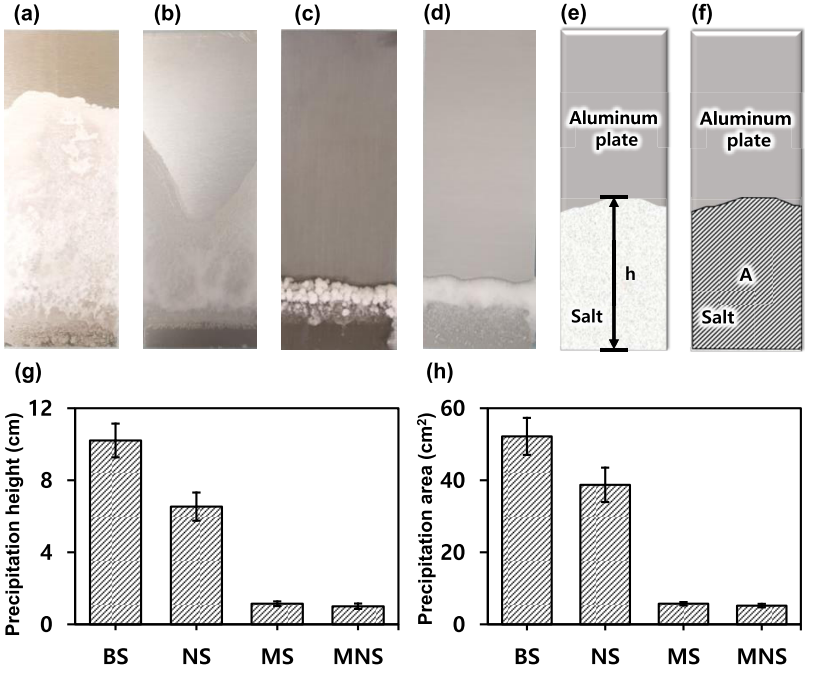

Figure 3. Precipitation experiment results on (a) bare surface, (b) nanostructured surface, (c) microstructured surface, and (d) micro/nanostructured surface. (e) Precipitation height measuring method; (f) precipitation area measuring method; (g) precipitation heights on the bare, nanostructured, microstructured, and micro/nanostructured surfaces; and (h) precipitation areas on the bare, nanostructured, microstructured, and micro/nanostructured surfaces.

showing the presence of Mg and O components (Figure 1f,h). This result can be verified by measuring the water CAs (WCAs). WCA refers to the angle formed by solid specimens and 5 μm deionized (DI) water droplets in the atmosphere at room temperature. The BS and MS of the aluminum oxide film with relatively low surface energy have high WCAs (Figure 1a,c), while the NS and MNS of aluminum hydroxide surface with high surface energy have very low WCAs (Figure 1b,d).

Precipitation Behavior of Different Surface Structures. An experiment was also conducted to observe the growth of salt precipitates on the BS, MS, NS, and MNS surfaces. The experiment was conducted for 144 h, and the precipitation process was observed every 24 h. On the BS (Figure 2a) and NS (Figure 2b) surfaces, NaCl particles are greatly spread out along the surface. In contrast, on the MS (Figure 2c) and MNS (Figure 2d) surfaces, the NaCl particles are thick and do not spread out significantly.

The precipitation height was measured to analyze the BS, NS, MS, and MNS surfaces (Figure 3a–d, respectively). The height of the precipitation spread was measured on the basis of the center line of the specimen, determined by the precipitation test results for each structure (Figure 3e). The

https://doi.org/10.1021/acsomega.1c05572
ACS Omega 2022, 7, 987−993

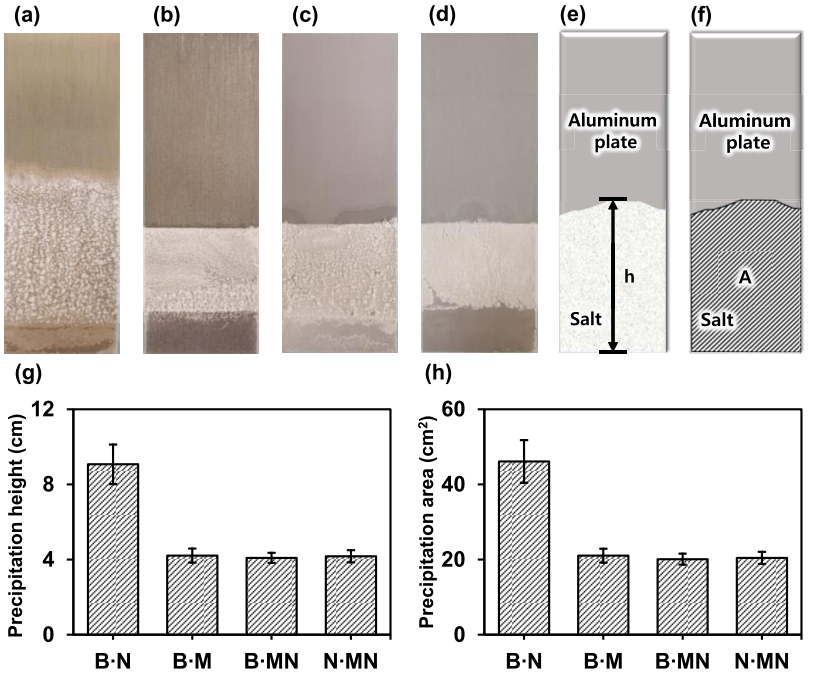

Figure 4. Precipitation experiment results on (a) bare·nanostructured surface, (b) bare·microstructured surface, (c) bare·micro/nanostructured surface, and (d) nano·micro/nanostructured surface. (e) Precipitation height measuring method; (f) precipitation area measuring method; (g) precipitation heights on the bare·nanostructured, bare·microstructured, bare·micro/nanostructured, and nano·micro/nanostructured surfaces; and (h) precipitation areas on the bare·nanostructured, bare·microstructured, bare·micro/nanostructured, and nano·micro/nanostructured surfaces.

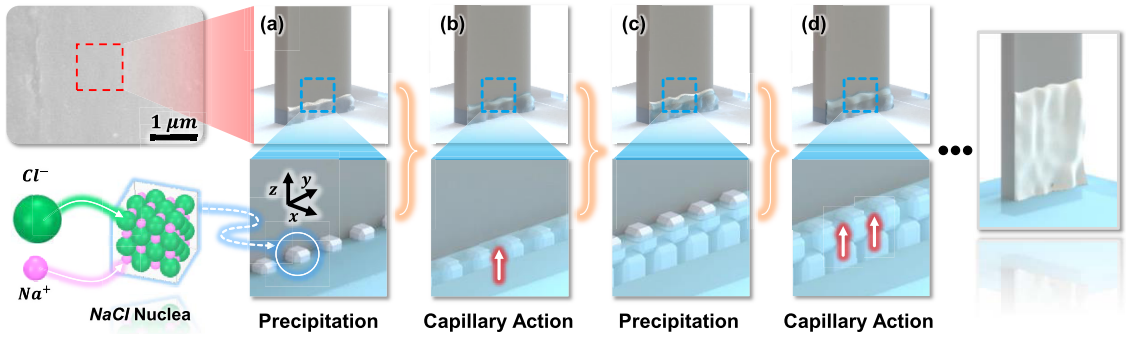

Figure 5. Three-dimensional schematic diagram of bare surface (BS) and nanostructured surface (NS) precipitation. (a) Precipitation on the boundary between the solution and the surface. (b) Capillary action in the space between crystals in the positive *z*-direction. (c) Precipitation on the changed boundary. (d) Capillary action in the space between new crystals in the positive *z*-direction.

area of the precipitation spread was measured through the image processing of the photos of precipitation test results for each structure (Figure 3f). The mean and standard deviation were calculated from the results of five repeated experiments (Figure 3g,h). The means and standard deviations of the precipitation heights on the BS, NS, MS, and MNS surfaces are 10.21 ± 0.94, 6.539 ± 0.78, 1.148 ± 0.13, and 1.003 ± 0.15 cm, respectively. The means and standard deviations of the precipitation areas on the BS, NS, MS, and MNS surfaces are 52.18 ± 5.15, 38.72 ± 4.78, 5.74 ± 0.45, and 5.21 ± 0.49 cm^2, respectively.

Precipitation Behavior of Patterned Surface Structures. Bare·nanostructured (B·N), bare·microstructured (B·M), bare·micro/nanostructured (B·MN), and nanostructured·micro/nanostructured (N·MN) patterned surfaces were manufactured using an acid-corrosion-resistant Kapton tape. The growth of salt precipitation on the patterned surfaces of B·N, B·M, B·MN, and N·MN was observed experimentally. The experiment was conducted for 144 h. As in the previous experiments, precipitation proceeded along the surface of the BS and NS; in contrast, it did not spread on the MS and MNS. On the B/N surface, the precipitation proceeds from the BS to the NS and the crystal growth continues (Figure 4a). On the remaining B·M (Figure 4b), B·MN (Figure 4c), and N·MN (Figure 4d) surfaces, the crystals do not spread because of the surface patterning boundary. The height of the precipitation spread was measured on the basis of the center line of the specimen, which was obtained from the precipitation test results for each structure (Figure 4e). The area of the precipitation spread was measured through the image processing of the photos of precipitation test results for each structure (Figure 4f). The mean and standard deviation were calculated from the results of five repeated experiments (Figure 4g,h). The means and standard deviations of the precipitation height on the B·N, B·M, B·MNS, and N·MNS surfaces are 9.071 ± 1.05, 4.213 ± 0.373, 4.049 ± 0.263, and 4.178 ± 0.324 cm, respectively. The means and standard deviations of the precipitation areas on the B·N, B·M, B·MNS, and N·MNS

https://doi.org/10.1021/acsomega.1c05572
ACS Omega 2022, 7, 987−993

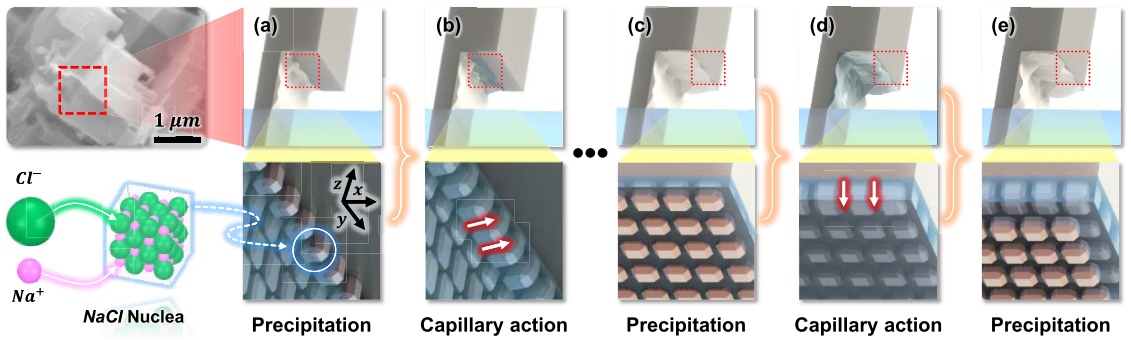

Figure 6. Three-dimensional schematic diagram of microstructured surface (MS) and micro/nanostructured surface (MNS) precipitation. (a) Precipitation on the boundary between the solution and the surface. (b) Capillary action in the space between crystals in the positive *x*-direction. (c) Precipitation on the changed boundary. (d) Capillary action in the space between new crystals in the negative *z*-direction. (e) Precipitation on the changed boundary.

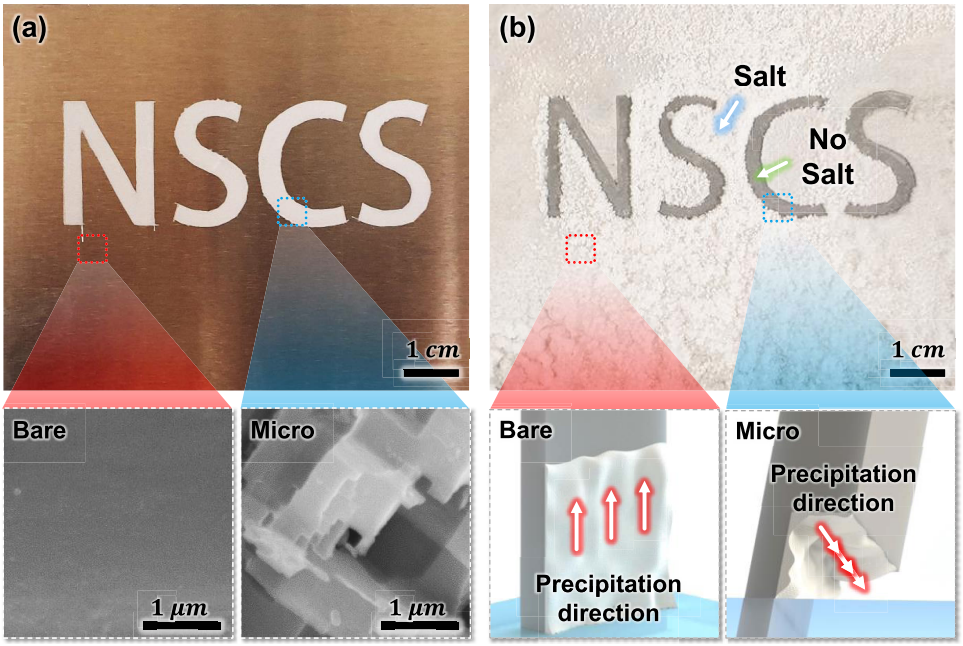

Figure 7. (a) Microsized structure patterning surface on the NSCS letter string. (b) Surface precipitation results after immersion in the saturated aqueous NaCl solution.

surfaces are 46.12 ± 5.69, 21.04 ± 1.87, 20.12 ± 1.45, and 20.45 ± 1.62 cm^2, respectively.

Hence, it can be concluded that the crystal growth behavior on BS and NS surfaces was different from that on MS and MNS surfaces with microcubic structures. In addition, the results revealed that the microstructure suppressed the spread of the crystals on the patterned surfaces.

According to the heterogeneous nucleation theory, precipitation by evaporation begins at the point where the aluminum surface meets the saturated aqueous NaCl solution. The surface tension of the saturated aqueous NaCl solution was 83.8 ± 0.28 mN/m, and the size of the nuclei produced therein has been reported to vary from several to tens of nanometers.[26] The precipitation process of BS and NS is shown in Figure 5. In the first step, numerous nuclei grow parallel to the surface boundary (Figure 5a). Then, a capillary force acts along the narrow gap between the grown nuclei, pulling the solution in the positive *z*-direction (Figure 5b). Afterward, similar to the first step, precipitation occurs at the interface (Figure 5c), and similar to the second step, a capillary action occurs in the positive *z*-direction (Figure 5d). The precipitation proceeds along the surface and involves a series of processes, and the crystal grows much higher than the original water level. Therefore, in BS and NS, the precipitation in the horizontal direction is much higher than that in the vertical direction of the aluminum surface.

MS and MNS with microcubic structures also begin to precipitate at the point where the aluminum surface and the saturated aqueous NaCl solution come into contact. The different precipitation results are attributed to the microcubic structure. The solution moves in the enlarged part because of the capillary force acting along the crystallized surface (Figure 6a). Because the capillary action acts in the positive *x*-direction, the boundary line of the solution can continue to move (Figure 6b). When this process is repeated and reaches the end of the microcubic structure (Figure 6c), the capillary force can no longer raise the solution in the positive *z*-direction, and gravity and capillary force act in the negative *z*-direction (Figure 6d). Therefore, the crystals can no longer rise upward and precipitate; instead, they thicken downward and

https://doi.org/10.1021/acsomega.1c05572
ACS Omega 2022, 7, 987−993

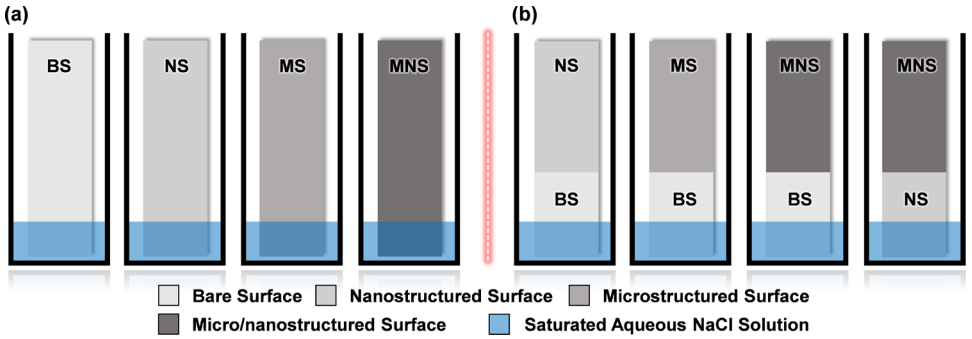

Figure 8. Schematic of the precipitation experiment using (a) surface structures and (b) patterning surface structures.

grow (Figure 6e). In other words, MS and MNS containing microstructures show much higher precipitation in the direction perpendicular to the surface than in the direction horizontal to the surface.

Finally, the results confirm that selective precipitation is possible using surface microstructures. In particular, a large structure on the order of several microns was found to influence the direction of the capillary phenomenon, thereby suppressing the width and height, as well as the spread, of the crystals. Therefore, it can be concluded that a flat surface induces the spreading of the precipitation, while a microstructured surface suppresses it.

CONCLUSIONS

This study showed that the precipitation phenomenon of a saturated aqueous NaCl solution can be controlled by modifying the surface structure. The industrial aluminum surface was modified to obtain nanostructured, microstructured, and micro/nanostructured surfaces. The structure, wettability, and elemental composition of each surface, including those of the bare surfaces, were analyzed, and precipitation experiments were conducted on the fabricated surfaces. While the precipitated crystals spread widely along the bare and nanostructured surfaces, the spread was inhibited on the microstructured and micro/nanostructured surfaces, which also contained microcubic structures.

The microscale structure of the surface suppresses crystal growth by preventing the solution from spreading along the surface. Patterning the microstructures on the surface can selectively allow or suppress precipitation along the patterned shape. For example, the microsized structure is patterned only on the letter string NSCS. After that, if it is immersed in the saturated aqueous NaCl solution, salt will be precipitated in all regions except for the NSCS region containing the microstructure, as shown in Figure 7. The study results provide a better understanding of the precipitation phenomenon at the solid−solution interface. Moreover, induction and inhibition of precipitation by changing the surface structure, which has been observed and described on the basis of our findings, is a novel functional phenomenon. In addition, the results of this study can suggest new possibilities to solve the pipe clogging problem by allowing selective precipitation by modifying the surface structure inside the tube.

EXPERIMENTAL SECTION

Materials. An aluminum sheet (99.5%, Chunwoo metal, Republic of Korea) was used as a material for preparing the experimental specimens. Sodium hydroxide (NaOH; 99.5%), sodium chloride (NaCl; 99.5%), hydrochloric acid (HCl; 35.0−37.0%), and ethyl alcohol (94.5%) were supplied by Samchun Chemical (Republic of Korea).

Methods. The surfaces used in the experiment were processed with aluminum to a width of 5 cm and a length of 15 cm. The bare surfaces (BS) were prepared by washing the untreated aluminum surface for 5 min using an ultrasonic cleaner in an ethanol environment. The nanostructured surfaces (NS) were prepared by immersing the washed aluminum surface in a 1 M NaOH aqueous solution at 25 °C for 1 min to remove surface impurities. To prepare the nanostructure using gelling aluminum, the aluminum surface was placed in boiling deionized (DI) water (over 90 °C) for 10 min and dried. The microstructured surfaces (MS) were prepared by immersing the washed aluminum surface in a 1 M HCl solution at 80 °C for 1 min to scrape the surface, followed by washing with DI water and drying. The micro/nanostructured surface (MNS) was prepared by shaping the microstructured surface with a HCl solution and immersing the washed surface in a 1 M NaOH aqueous solution at 25 °C for 5 s to gelate the surface, placing it in boiling DI water (over 90 °C) for 10 min, followed by drying.

Surface Precipitation. A glass beaker (Corning) was used for all surface precipitation experiments. A constant-temperature-and-humidity chamber (SH SCIENTIFIC, Republic of Korea) was used to maintain the experimental environment. A forced circulation dryer (SH SCIENTIFIC) was used to dry each surface. The prepared aluminum surfaces were dried at 60 °C for 5 min for all surface precipitation experiments. A saturated NaCl solution was prepared by mixing NaCl and water (0.359:1 m/m). An experiment was conducted to observe the crystal growth process for each surface. The BS, NS, MS, and MNS and a saturated aqueous NaCl solution were prepared. Under the same temperature and humidity conditions, each surface was first immersed 15 mm below the surface in 120 mL of a saturated aqueous NaCl solution, and then the crystallization process was observed by periodically photographing the growth of crystals on the surface (Figure 8a,b).

Characterization. Field-emission scanning electron microscopy (FE-SEM; SU6600, Hitachi, Japan) was used to examine the surface morphologies, and energy-dispersive spectroscopy−electron backscatter diffraction (EDS−EBSD; Pegasus, EDAX) was used to examine the surface elemental composition. CAs were measured using a CA analyzer (SmartDrop, Femtofab Co., Republic of Korea), on the basis of the averages of five experiments conducted using 5 μL droplets. A digital caliper (CAS, Republic of Korea) was used to measure the precipitation height.

https://doi.org/10.1021/acsomega.1c05572
ACS Omega 2022, 7, 987−993

■ ASSOCIATED CONTENT

Supporting Information

The Supporting Information is available free of charge at https://pubs.acs.org/doi/10.1021/acsomega.1c05572.

Schematics design of homogeneous nucleation and schematics design of heterogeneous nucleation (PDF)

■ AUTHOR INFORMATION

Corresponding Authors

Jeong-Won Lee − *Department of Mechanical Engineering, Chosun University, Gwangju 61452, Republic of Korea;* orcid.org/0000-0001-9207-7678; Phone: 82-62-230-7058; Email: jwlee07@chosun.ac.kr; Fax: 82-62-608-5233

Woonbong Hwang − *Department of Mechanical Engineering, Pohang University of Science and Technology, Pohang, Gyeongbuk 37673, Republic of Korea;* orcid.org/0000-0001-9072-9732; Phone: 82-54-279-2174; Email: whwang@postech.ac.kr; Fax: 82-54-279-5899

Authors

Kihwan Kim − *Department of Mechanical Engineering, Pohang University of Science and Technology, Pohang, Gyeongbuk 37673, Republic of Korea*

Kwangseok Lee − *Department of Mechanical Engineering, Pohang University of Science and Technology, Pohang, Gyeongbuk 37673, Republic of Korea*

Jaehyun Choi − *LG Innotek, Seoul 07796, Republic of Korea*

Complete contact information is available at: https://pubs.acs.org/10.1021/acsomega.1c05572

Notes

The authors declare no competing financial interest.

■ ACKNOWLEDGMENTS

This work was financially supported by the National Research Foundation of Korea (NRF) grant funded by the Korea government (MSIT) (NRF-2021R1A2C2008600).

■ REFERENCES

(1) Sedivy, V. M. Environmental Balance of Salt Production Speaks in Favour of Solar Saltworks. *Global NEST J.* **2009**, *11*, 41−48.

(2) Swain, B. Recovery and recycling of lithium: A review. *Sep. Purif. Technol.* **2017**, *172*, 388−403.

(3) An, J. W.; Kang, D. J.; Tran, K. T.; Kim, M. J.; Lim, T.; Tran, T. Recovery of lithium from Uyuni salar brine. *Hydrometallurgy* **2012**, *117−118*, 64−70.

(4) Azamathulla, H. M.; Ahmad, Z. Estimation of Critical Velocity for Slurry Transport through Pipeline Using Adaptive Neuro-Fuzzy Interference System and Gene-Expression Programming. *J. Pipeline Syst. Eng. Pract.* **2013**, *4*, 131−137.

(5) Janda, A.; Zuriguel, I.; Garcimartín, A.; Maza, D. Clogging of granular materials in narrow vertical pipes discharged at constant velocity. *Granular Matter* **2015**, *17*, 545−551.

(6) Steinhagen, R.; MÜLler-Steinhagen, H.; Maani, K. Problems and Costs due to Heat Exchanger Fouling in New Zealand Industries. *Heat Transfer Eng.* **1993**, *14*, 19−30.

(7) Müller-Steinhagen, H.; Malayeri, M. R.; Watkinson, A. P. Heat Exchanger Fouling: Mitigation and Cleaning Strategies. *Heat Transfer Eng.* **2011**, *32*, 189−196.

(8) Elliot, M. N. The Present State of Scale Control in Sea Water Evaporators. *Desalination* **1969**, *6*, 87−104.

(9) Sayari, S.; Mahdavi-Meymand, A.; Zounemat-Kermani, M. Prediction of Critical Velocity in Pipeline Flow of Slurries Using TLBO Algorithm: A Comprehensive Study. *J. Pipeline Syst. Eng. Pract.* **2020**, *11*, No. 04019057.

(10) Semenenko, Y.; Kril, S.; Medvedieva, O.; Nykyforova, N.; Tatarko, L. Calculation of pressure loss and critical velocity for slurry flows with additive agents in vertical polyethylene pipelines. *E3S Web Conf.* **2019**, *109*, No. 00083.

(11) Fisher, J. C.; Hollomon, J. H.; Turnbull, D. Nucleation. *J. Appl. Phys.* **1948**, *19*, 775−784.

(12) Wenzel, R. N. Resistance of Solid Surfaces to Wetting by Water. *Ind. Eng. Chem.* **1936**, *28*, 988−994.

(13) Dai, X.; Stogin, B. B.; Yang, S.; Wong, T. S. Slippery Wenzel State. *ACS Nano* **2015**, *9*, 9260−9267.

(14) Kim, K.; Lee, K.; Choi, J.; Hwang, W. A Study on the Drag Reduction Performance and NaCl Solution Robustness according to the Wetting Characteristics of Bottom Surface of Water Vehicle. *J. Korean Soc. Precis. Eng.* **2020**, *37*, 297−303.

(15) Jun, G.; Lee, J. W.; Shin, Y.; Kim, K.; Hwang, W. Solvent-aided direct adhesion of a metal/polymer joint using micro/nano hierarchical structures. *J. Mater. Process. Technol.* **2020**, *285*, No. 116744.

(16) Kim, S.; Kim, K.; Jun, G.; Hwang, W. Wood-Nanotechnology-Based Membrane for the Efficient Purification of Oil-in-Water Emulsions. *ACS Nano* **2020**, *14*, 17233−17240.

(17) Lee, J. W.; Kim, S.; Lee, S.; Hwang, W. Exponential promotion and suppression of bubble nucleation in carbonated liquid by modification of surface wettability. *Appl. Surf. Sci.* **2020**, *512*, No. 145709.

(18) Lee, K.; Lee, J. W.; Kim, K.; Yoo, D.; Kim, D. S.; Hwang, W.; Song, I.; Sim, J. Y. A Spherical Hybrid Triboelectric Nanogenerator for Enhanced Water Wave Energy Harvesting. *Micromachines* **2018**, *9*, No. 598.

(19) Ji, D.-Y.; Lee, J.-W.; Hwang, W.; Lee, K.-Y. Experimental study of condensation heat transfer on a horizontal aluminum tube with superhydrophobic characteristic. *Int. J. Heat Mass Transfer* **2019**, *134*, 286−295.

(20) Rose, J. W. Dropwise condensation theory and experiment: A review. *Proc. Inst. Mech. Eng., Part A* **2002**, *216*, 115−128.

(21) Nath, S.; Ahmadi, S. F.; Boreyko, J. B. A Review of Condensation Frosting. *Nanoscale Microscale Thermophys. Eng.* **2017**, *21*, 81−101.

(22) Wang, H.; Tang, L.; Wu, X.; Dai, W.; Qiu, Y. Fabrication and anti-frosting performance of super hydrophobic coating based on modified nano-sized calcium carbonate and ordinary polyacrylate. *Appl. Surf. Sci.* **2007**, *253*, 8818−8824.

(23) Rees, W. S., Jr Thin Film Nucleation, Growth, and Microstructural Evolution. In *Handbook of Deposition Technologies for Films and Coatings*, 3rd ed., Martin, P. M., Noyes, Park Ridge, 2010; pp 554−620.

(24) Röpke, G.; Priezzhev, V. B. Nucleation and Crystallization Kinetics in Silicate Glasses: Theory and Experiment. In *Nucleation Theory and Applications*, 1st ed., Schmelzer, J. W. P., Wiley-VCH AA, Weinheim, 2005; pp 78−79.

(25) Batchelor, G. K. *An Introduction to Fluid Dynamics; Cambridge Mathematical Library*, Cambridge University Press, Cambridge, 2000.

(26) Nakamuro, T.; Sakakibara, M.; Nada, H.; Harano, K.; Nakamura, E. Capturing the Moment of Emergence of Crystal Nucleus from Disorder. *J. Am. Chem. Soc.* **2021**, *143*, 1763−1767.